Reduction of scattering loss in fluoroindate glass fibers

Jiafang Bei,[1,*] Tanya M. Monro,[1] Alexander Hemming,[2] and Heike Ebendorff-Heidepriem[1]

[1]*Institute for Photonics and Advanced Sensing and School of Chemistry and Physics, University of Adelaide, Adelaide, SA 5005, Australia*

[2]*Electro-Optic Technology Group, Electronic Warfare and Radar Division, Defence Science and Technology Organisation, Edinburgh, SA 5111, Australia*

**jiafang.bei@adelaide.edu.au*

Abstract: The current fluoroindate glass optical fiber loss is dominated by extrinsic absorption and scattering loss. Attempts were made to reduce fluoroindate glass fiber loss by optimizing glass melting conditions, preform extrusion process and fiber drawing conditions. Our results show that fluorination of the glass batches (with 99.99% InF_3) at 450 °C by addition of ammonium bifluoride reduced un-dissolved particles (potential scattering losses) in the glass. Glass flow analysis was carried out to provide insights into the glass temperature-viscosity behavior and the relationship between preform surface roughness and extrusion temperature, which enabled fabrication of preforms with low surface roughnesses and eventually reduced the fiber scattering loss. Fiber surface crystallization was reduced via conducting chemical etching and polishing (with colloidal silica) on both glass billets and preforms, extending the heating zone for fiber drawing, and applying additional weight at the bottom of preforms. As a consequence, the fiber surface roughness decreased, resulting in decreased fiber scattering loss and enhanced fiber strength.

OCIS codes: (160.2290) Fiber materials; (160.2750) Glass and other amorphous materials.

References and links

1. X. Zhu and N. Peyghambarian, "High-power ZBLAN glass fiber lasers: Review and prospect," Adv. Optoelectron. **2010**, 501956 (2010).
2. M. Saad, "Fluoride glass fiber: state of the art," Proc. SPIE **7316**, 73160N, 73160N-16 (2009).
3. S. Shibata, M. Horiguchi, K. Jinguji, S. Mitachi, T. Kanamori, and T. Manabe, "Prediction of loss minima in infra-red optical fibers," Electron. Lett. **17**(21), 775–777 (1981).
4. T. Kanamori and S. Sakaguchi, "Preparation of elevated NA fluoride optical fibers," Jpn. J. Appl. Phys. **25**(Part 2, No. 6), L468–L470 (1986).
5. J. Lucas, "Fluoride glasses," J. Mater. Sci. **24**(1), 1–13 (1989).
6. S. Mitachi, Y. Terunuma, Y. Ohishi, and S. Takahashi, "Reduction of impurities in fluoride glass fibers," J. Lightwave Technol. **2**(5), 587–592 (1984).
7. G. F. West and W. Höfle, "Spectral attenuation of fluoride glass fibers," J. Non-Cryst. Solids **213–214**, 189–192 (1997).
8. P. C. Pureza, P. H. Klein, W. I. Roberts, and I. D. Aggarwal, "Influence of preform surface treatments on the strength of fluorozirconate fibers," J. Mater. Sci. **26**(19), 5149–5154 (1991).
9. J. Bei, T. M. Monro, A. Hemming, and H. Ebendorff-Heidepriem, "Fabrication of extruded fluoroindate optical fibers," Opt. Mater. Express **3**(3), 318–328 (2013).
10. A. M. Mailhot, A. Elyamani, and R. E. Riman, "Reactive atmosphere synthesis of Sol-gel heavy metal fluoride glasses," J. Mater. Res. **7**(06), 1534–1540 (1992).
11. S. Takahashi, T. Kanamori, Y. Ohishi, K. Fujiura, and Y. Terunuma, "Reduction of oxygen impurity in ZrF_4-based fluoride glass," Mater. Sci. Forum **32–33**, 87–92 (1988).
12. R. M. Almeida and J. D. Mackenzie, "The effects of oxide impurities on the optical properties of fluoride glasses," J. Non-Cryst. Solids **56**(1-3), 63–68 (1983).
13. Y. Nishida, T. Kanamori, T. Sakamoto, Y. Ohishi, and S. Sudo, "Fluoride glass fiber," U. S. Patent 5 774 620, June 30, 1998.

#192346 - $15.00 USD Received 17 Jun 2013; revised 3 Aug 2013; accepted 4 Aug 2013; published 13 Aug 2013

14. Y. Nishida, T. Kanamori, T. Sakamoto, Y. Ohishi, and S. Sudo, "Development of PbF_2-GaF_3-InF_3-ZnF_2-YF_3-LaF_3 glass for use as a 1.3 μm Pr^{3+}-doped fiber amplifier host," J. Non-Cryst. Solids **221**(2-3), 238–244 (1997).
15. Y. Jestin, A. L. Sauze, B. Boulard, Y. Gao, and P. Baniel, "Viscosity matching of new PbF2-InF3-GaF3 based fluoride glasses and ZBLAN for high NA optical fiber," J. Non-Cryst. Solids **320**(1-3), 231–237 (2003).
16. H. Ebendorff-Heidepriem and T. M. Monro, "Analysis of glass flow during extrusion of optical fiber preforms," Opt. Mater. Express **2**(3), 304–320 (2012).
17. E. Roeder, "Extrusion of glass," J. Non-Cryst. Solids **5**(5), 377–388 (1971).
18. H. Ebendorff-Heidepriem, Y. Li, and T. M. Monro, "Reduced loss in extruded soft glass microstructured fiber," Electron. Lett. **43**(24), 1343–1345 (2007).
19. H. Ebendorff-Heidepriem and T. M. Monro, "Extrusion of complex preforms for microstructured optical fibers," Opt. Express **15**(23), 15086–15092 (2007).
20. H. Ebendorff-Heidepriem, T.-C. Foo, R. C. Moore, W. Zhang, Y. Li, T. M. Monro, A. Hemming, and D. G. Lancaster, "Fluoride glass microstructured optical fiber with large mode area and mid-infrared transmission," Opt. Lett. **33**(23), 2861–2863 (2008).
21. H. W. Schneider, A. Schoberth, A. Staudt, and C. Gerndt, "Fluoride glass etching method for preparation of infra-red fibers with improved tensile strength," Electron. Lett. **22**(18), 949–950 (1986).
22. I. D. Aggarwal and G. Lu, *Fluoride Glass Fiber Optics* (Academic Press, 1991), Chap. 5.
23. G. Qian, F. Xia, J. Brugger, W. M. Skinner, J. Bei, G. Chen, and A. Pring, "Replacement of pyrrhotite by pyrite and marcasite under hydrothermal conditions up to 220 °C: An experimental study of reaction textures and mechanisms," Am. Mineral. **96**(11-12), 1878–1893 (2011).
24. Y. Ahn, J.-Y. Yoon, C.-W. Baek, and Y.-K. Kim, "Chemical mechanical polishing by colloidal silica-based slurry for micro-scratch reduction," Wear **257**(7-8), 785–789 (2004).
25. H. Ebendorff-Heidepriem, T. C. Foo, R. C. Moore, W. Zhang, Y. Li, T. M. Monro, A. Hemming, and D. G. Lancaster, "Fluoride glass microstructured optical fiber with large mode area and mid-infrared transmission," Opt. Lett. **33**(23), 2861–2863 (2008).
26. G. Rault, J. L. Adam, F. Smektala, and J. Lucas, "Fluoride glass compositions for waveguide applications," J. Fluor. Chem. **110**(2), 165–173 (2001).
27. C. Voyce, A. D. Fitt, and T. M. Monro, "Mathematical modeling as an accurate predictive tool in capillary and microstructured fiber manufacture: the effects of preform rotation," J. Lightwave Technol. **26**(7), 791–798 (2008).
28. S. Sakaguchi, Y. Terunuma, Y. Ohishi, and T. Kanamori, "Fluoride fiber drawing with improved tensile strength," J. Mater. Sci. Lett. **6**(9), 1063–1065 (1987).
29. P. W. France, *Fluoride Glass Optical Fibers* (Blackie, 1990), Chap. 9.
30. M. Saad, "High purity fluoride glass synthesis: a review" (IR photonics 2009). *http://www.iguide-irphotonics.com/pdf/Pwest2009.pdf*.
31. M. Braglia, S. Mosso, G. Dai, E. Billi, L. Bonelli, M. Baricco, and L. Battezzati, "Rheology of tellurite glasses," Mater. Res. Bull. **35**(14-15), 2343–2351 (2000).
32. E. Roeder, "Flow behaviour of glass during extrusion," J. Non-Cryst. Solids **7**(2), 203–220 (1972).
33. J. E. Shelby, *Introduction to Glass Science and Technology* (The Royal Society of Chemistry, 2005), Chap. 6.
34. H. Ebendorff-Heidepriem, T. M. Monro, M. A. van Eijkelenborg, and M. C. J. Large, "Extruded high-NA microstructured polymer optical fiber," Opt. Commun. **273**(1), 133–137 (2007).
35. E. W. Deeg, C. G. Silverberg, and L. B. Martel, "Method for fire polishing optical glass," U. S. Patent 3 811 857, May 21, 1974.
36. Jr. J. E. Dickinson and B. R. Wheaton, "Processes for polishing glass and glass-ceramic surfaces using excimer laser radiation," U. S. Patent 5 742 026, April 21, 1998.
37. P. A. Thompson and S. M. Troian, "A general boundary condition for liquid flow at solid surfaces," Nature **389**(6652), 360–362 (1997).
38. K. M. Reich, C. V. Gay, and J. A. Frangos, "Fluid shear stress as a mediator of osteoblast cyclic adenosine monophosphate production," J. Cell. Physiol. **143**(1), 100–104 (1990).
39. M. Chatzimina, G. C. Georgiou, K. Housiadas, and S. G. Hatzikiriakos, "Stability of the annular Poiseuille flow of a Newtonian liquid with slip along the walls," J. Non-Newton. Fluid Mech. **159**, 1–9 (2009).
40. D. R. MacFarlane, P. J. Newman, and A. Voelkel, "Methods of purification of zirconium tetrafluoride for fluorozirconate glass," J. Am. Ceram. Soc. **85**(6), 1610–1612 (2002).

1. Introduction

Fluoride glasses have attracted much interest as potential materials for high power fiber delivery in the mid-infrared spectral region due to their unique optical properties [1]. They show a wide transmission range from the ultraviolet to the mid-infrared region, and have significantly lower theoretical optical loss than that of conventional silicate glass fibers [2]. Shibata et al. estimated the theoretical minimum fluoride fiber loss to be $<10^{-2}$ dB/km at 2-3 μm, one magnitude lower than that of silica fiber. This estimate was based on losses due to

#192346 - $15.00 USD Received 17 Jun 2013; revised 3 Aug 2013; accepted 4 Aug 2013; published 13 Aug 2013

Rayleigh scattering and IR edge absorption which are the dominant intrinsic loss factors in fluoride glasses [3]. However, the losses of fabricated fluoride fibers are higher than the theoretically estimated value. It is important to note that Rayleigh scattering, which ultimately determines the attainable loss, represents only a small contribution to the fiber loss for fibers fabricated to date, and elimination of many other extrinsic losses caused by absorptions and scatterings are challenging. The lowest fiber loss reported so far is 0.7 dB/km at 2.6 μm measured by Kanamori and Sakaguchi on a 30 m long fluorozirconate fiber [4], which is still higher than the theoretical loss. Since fluoride glasses have significantly lower crystallization stability than oxide glasses, impurities in the raw materials and moisture in the atmosphere during preparation of fluoride glasses can easily induce crystallization which leads to scattering centers and increases the loss [5]. Absorption of impurities such as transition metals and rare earth ions in the raw materials also contributes to the loss of the glass, resulting in absorption losses in the fibers [6].

Many researchers have reported efforts towards the development of low-loss fluoride glass fibers by reducing sources of extrinsic absorption and scattering. Hydroxyl ion, transition metals and rare earth elements in the raw materials, which result in absorption loss in glass fibers, are major problems to be overcome in the production of ultra-low loss fluoride glass fibers. Defects that cause scattering can be divided into volume and surface defects. Volume defects (e.g., contaminations from platinum crucible, bubbles, un-dissolved particles and crystals [7]) are imperfections within the glass matrices that are principally formed during glass melting. Surface defects (e.g., surface contaminations, micro-cracks, scratches [8] and surface crystallization) originate from the contact of the glass surfaces with molds or extrusion dies during casting and extrusion [9] and from the reaction of the glass surface with moisture in the atmosphere during fiber fabrication or storage.

The first step in reducing extrinsic losses in these glasses is to reduce oxide impurities in the starting materials used for the glass melts. This is achieved using a fluorination process during the glass melting, which can reduce the concentration of oxide impurities in the glasses [6,10], resulting in reduced scattering in the glasses. One traditional approach to fluorination is the use of ammonium bifluoride (NH_4HF_2) during glass synthesis to fluorinate all non-fluoride impurities in the raw materials [11]. In particular, this method plays a critical role in reducing the content of oxides and oxy-hydrides, which would otherwise increase the IR absorption or shorten the IR cut-off wavelength and result in substantial loss in the glasses [12].

In principle, by conducting all glass preparation under fluorination with ammonium bifluoride, the level of oxides and oxy-hydrides can be significantly reduced. However, other sources of extrinsic loss such as bubbles and poor surface quality (caused by e.g., surface crystallization) will cause an increase in fiber loss. Hence, it is critical to reduce loss in fluoride fibers by improving preform and fiber fabrication conditions. Casting techniques (e.g., rotational casting and suction casting methods) have been used successfully for preparation of fluoride glass preform and fluoroindate glass fibers [13–15]. An alternative technique is billet extrusion, which can be used to form long preforms of a desired diameter as well as a range of internal structures [16,17]. Compared to the casting method, the extrusion technique is a versatile method for the production of low-loss microstructured optical fibers with various shapes produced from different types of glasses [18–20]. It also has been demonstrated that the extrusion method is suitable for the preparation of bubble-free rods, which typically exhibit better surface finish and fewer bubbles than cast rods [9]. However, both casting and extrusion methods unavoidably introduce surface contaminations (i.e., metallic particles and graphite particles) and surface scratches (leading to high roughness) generated during contact with molds or dies. Poor surface quality associated with these surface contaminations and scratches will cause low fiber strength and high loss in air-clad (i.e., unstructured) fibers and air/glass microstructured fibers unless the contaminated layer can be removed [8]. The surface quality can be improved by chemical etching, which allows a uniform and rapid dissolution of surface

#192346 - $15.00 USD Received 17 Jun 2013; revised 3 Aug 2013; accepted 4 Aug 2013; published 13 Aug 2013

regions in fluoride glasses. The etching method can also smooth the fiber surface (i.e., reduce the surface roughness), which enables the preparation of fluoride fibers with low transmission loss and high fiber strength [21]. Although chemical etching prior to fiber drawing can effectively remove defects on the preform surface, fiber preform drawing presents a new set of challenges such as precise control of temperature and atmosphere. Since the viscosity of fluoride glasses shows a strong temperature dependence and sensitivity to surrounding atmosphere, an accurate control of the drawing temperature and atmosphere is critical to the preparation of long-length, low-loss and high-strength fibers [8,22].

In our previous study [9], the extrusion technique was demonstrated to be a suitable method for the production of low loss fluoroindate fibers made from $32InF_3$-$20ZnF_2$-$20SrF_2$-$18BaF_2$-$8GaF_3$-$2CaF_2$ (IZSBGC) glass. This fluoroindate glass composition is particularly promising for applications in the mid-infrared spectral region due to its high transmission and relatively low rate of crystallization compared to ZBLAN glass [9]. However, the presence of surface crystallization (e.g., white precipitates) and roughness on the preforms, which were major scattering centers, caused high fiber loss and low fiber strength in our previous work [9]. The aim of this study is therefore to reduce the fiber scattering loss and to improve mechanical strength of unstructured fibers by minimizing surface crystallization and roughness through optimization of fluorination processes, extrusion and fiber drawing conditions.

2. Experimental conditions and measurement techniques

2.1 Glass melting

All glass fabrication steps including weighing of the raw materials (batching), fluorination at 235 °C (45 min) or 450 °C (1 h), melting at 900 °C for 2 or 3 h, and casting were conducted in a controlled dry N_2 atmosphere (99.99%) melting facility. The temperature ramp speed was set to 5 °C/min. The glasses were prepared using commercially available fluorides as starting materials which were thoroughly mixed into 30-130 g batches and then melted in a platinum alloy crucible containing 5% gold (internal volume: 100 or 300 ml). We used two different InF_3 raw materials: 99.99% (metal purity) $InF_3{\cdot}3H_2O$ (labeled with a star '*' in Table 1), and anhydrous 99.99% (metal purity) InF_3 (labeled with double star '**' in Table 1). To fluorinate oxide impurities in the batch, NH_4HF_2 was added to the batch before melting. However, H_2O in $InF_3{\cdot}3H_2O$ reacts with InF_3, resulting in $In(OH)_3$ and gaseous HF. Hence, for glass batches using $InF_3{\cdot}3H_2O$, a higher amount of excess NH_4HF_2 (6.7 wt% of the batch weight) was used to compensate the loss of fluorine due to the formation and loss of HF, while for glass batches containing anhydrous InF_3 a lower amount of NH_4HF_2 was used (2.4 wt% of the batch weight) due to higher fluorine content in the raw material. The glass batches were first fluorinated at 235 °C or 450 °C, followed by melting at 900 °C. Finally, the glass melts were cast into a pre-heated mold. For basic glass characterization (samples A-C in Table 1), small melts of ~30 g were cast into rectangular glass blocks of dimensions of 15×10×30 mm^3. For preform extrusion, larger glass melts (up to 130 g) were prepared and cast into a cylindrical mold, resulting in glass billets of 30 mm diameter and 20-30mm height.

2.2 Chemical etching and mechanical polishing

To improve the surface quality of the cast billets and extruded preforms, mechanical polishing and/or chemical etching surface treatments were applied. More specifically, after glass melting, cylindrical billets were polished using 3 μm diamond pastes and then suspensions of 40 nm colloidal silica, which produced scratch-free surfaces [23,24]. For comparison purposes, some of the billets and/or preforms for chemical etching were suspended in a 1.36 M $ZrOCl_{2(aq)}$ solution (with stirring applied) at room temperature for about 30 min to remove a ~0.5 mm thick outer layer, followed by a rinse in methanol in an ultrasonic bath for 30 min and final hand polishing with 40nm colloidal silica solution (hereafter referred to as

#192346 - $15.00 USD Received 17 Jun 2013; revised 3 Aug 2013; accepted 4 Aug 2013; published 13 Aug 2013

chemo-mechanical treatment). The published etching solution recipe, i.e., 0.4 mol $ZrOCl_2 \cdot 8H_2O$ in 1L 1N HCl for ZBLAN glasses [21] resulted in the formation of a white layer on a glass preform during etching. However, when a 1.36 M $ZrOCl_{2(aq)}$ solution (optimized concentration) was used, white layer was not observed on the preform (immersed in etching solution) during the etching process. After etching, the preform was rinsed with methanol for 30 min and then was dried out using a N_2 gas gun. A few regions of light white layers were, however, found on the dried and etched billet or preform surface. Hence, we polished etched billets or preforms with a 40 nm colloidal silica suspension to remove white layer formed during etching. In comparison with our previous work, etching with 15 wt% $HCl_{(aq)}$ solution resulted in a significant white layer giving rise to a high loss [9].

2.3 Extrusion

Billet extrusion technique has been demonstrated as a suitable method for fluoroindate glass preform fabrication [9]. Extrusion conditions for fluorindate glasses were based on previous work on fluorozirconate glass extrusion [20]. Graphite has been successfully used as a die material for fluorozirconate glass extrusion due to the relatively low friction between the die and glass surfaces. Fluorozirconate glass could be extruded at a higher viscosities (~10^8 Pa·s), i.e., lower temperatures, using a graphite die compared with a stainless steel die. Extrusion with a graphite die allowed fluorozirconate preforms to be extruded below the onset of glass surface crystallization temperature (290 °C [25]) which is 62 °C lower than the glass crystallization temperature measured by DSC (T_x = 352 °C [26]). In this work, graphite was also used as the die material for the extrusion of IZSBGC glass at a temperature below the onset of glass crystallization temperature [9,20]. Surface crystallization of IZSBGC glass was observed for a 330 °C extrusion temperature, which is ~60 °C lower than T_x = 389 °C determined by DSC in our previous work [9]. Therefore, following polishing or chemo-mechanical treatment, the cylindrical billets were extruded into rod-shape (cylindrical) preforms of 5-10 mm in diameter at temperatures in the range of the glass transition temperature (T_g = 307 °C) (Fig. 2) to T_g + 23 °C under N_2 controlled atmosphere. Four types of graphite dies (a-d) with different die channel lengths and diameters (Table 2) were used to extrude unstructured rods. Die types (a) (8 mm die channel diameter) and (d) (5 mm die channel diameter) were used for the extrusion of 65 g (batch weight) glass billets, whereas die types (b) and (c) were used for extrusion of ≥100 g (batch weight) glass billets.

The extrusion trials were conducted at a fixed temperature and ram speed, while the extrusion force was varied. For the calculations described in Section 3.2, we used the extrusion force applied after the die was completely filled with glass, i.e., when the rod started to emerge from the extrusion die (Fig. 1). The other details of the extrusion set-up, die types and error analysis used in this work can be found in [16]. For analysis of the extrusion data in Table 2, errors for the viscosity values were obtained based on relative errors for the temperature measurements (0.90-0.95%) and ram force, *F* (3-17% in the region when a rod emerged from a die).

#192346 - $15.00 USD Received 17 Jun 2013; revised 3 Aug 2013; accepted 4 Aug 2013; published 13 Aug 2013

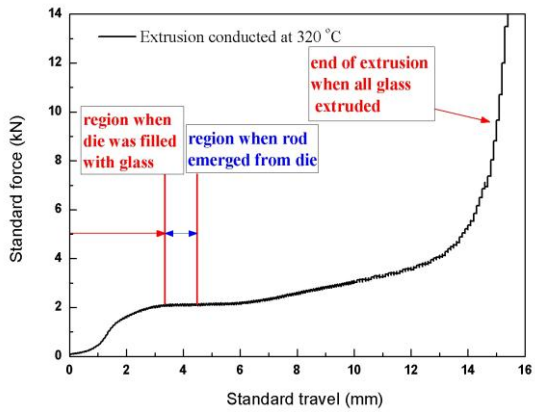

Fig. 1. Extrusion force profile for a fluoroindate extrusion trial using die (c) at 320 °C.

2.4 Fiber drawing

All preforms were pulled into unstructured fibers with diameters ranging from 130 to 180 μm under N_2 controlled atmosphere. The induction heating furnace used in the fiber drawing tower comprises a cylindrical graphite ring, which acts as the susceptor and therefore the heat source of the furnace. In a fiber-drawing furnace, the temperature that controls the furnace temperature is usually measured at a point close to the heat source (in our case the susceptor). However, earlier studies showed that the glass temperature varied significantly along the length of the furnace and also depended upon the heat source length [27,28], which corresponds to susceptor length for our fiber drawing furnace. Two types of graphite susceptors with the same inner and outer diameters but different heights (2 cm or 4.5 cm-long) were used to explore the impact of the furnace working temperature and the maximum preform temperature for fluoroindate glass fiber fabrications. For some preforms, an additional weight of ~190 g was applied to the bottom of the preforms during fiber drawing to decrease the temperature at which a drop is formed, thereby reducing the surface crystallization on the preform.

2.5 Measurements

The characteristic temperatures, i.e., glass transition temperature (T_g), glass crystallization temperature (T_x) and peak of crystallization temperature (T_p), of samples A and C (Fig. 2) were measured using a Setaram Differential Scanning Calorimetry (DSC) 131 equipment with experimental errors of ± 2 °C. This measurement was conducted from room temperature up to 530 °C at a heating rate of 10 °C /min under N_2 atmosphere.

For thermal dilatometric measurement, we used a piece of 5 mm diameter rod that was extruded at 320 °C. This measurement was conducted from room temperature up to 500 °C at a heating rate of 5 °C/min using a Dilatometer (Netzsch DIL 402, Germany), with experimental errors of ± 0.01 °C.

The surface roughness of preforms and fibers were measured using an optical interferometric profiler (model Contour GT-K1 Optical Profiler Stitching System from Veeco). From the optical profiler images, roughness parameters, S_a (average roughness), and S_q (root mean square (RMS) roughness) defined in Eqs. (4) and (5), respectively [9], were determined using the following expressions

$$S_a = \frac{1}{MN}\sum_{k=0}^{M-1}\sum_{l=0}^{N-1}\left|z(x_k, y_l)\right| \tag{1}$$

#192346 - $15.00 USD Received 17 Jun 2013; revised 3 Aug 2013; accepted 4 Aug 2013; published 13 Aug 2013

$$S_q = \sqrt{\frac{1}{MN}\sum_{k=0}^{M-1}\sum_{l=0}^{N-1}\left[z(x_k, y_l)\right]^2} \quad (2)$$

where M and N are the numbers of the measured points and $Z(x_k, y_l)$ is the distance from each measured point to the central plane on the surface of the tested preform sample. Three surfaces areas, each being ~120×160 μm^2, were probed in the preforms, while five areas, each being ~25×160 μm^2, were measured in the fibers.

To investigate the impact of fabrication conditions on fiber loss, we selected 1550 nm as a wavelength for spot loss measurements and broadband spectral range of 500-1750 nm for white light source measurements. The fiber losses were measured based on the cutback method using a 1550 nm laser (spot loss measurement) and a bulb (broadband loss measurement) as the light sources. The output power of the fiber under test during spot loss measurement at 1550 nm was recorded by a power meter and for broadband loss measurement with an optical spectrum analyzer. The relative errors for spot loss measurements varied from 2.2% to 5.9% of the average value. The uncertainties of the broadband loss measurements were up to 10% of measured values.

The mid-IR fiber transmission was measured from 2 to 8 μm using a fiber-coupled Bruker Vertex 70 FTIR spectrometer with a liquid nitrogen cooled HgCdTe detector. The fiber loss was determined via a cut-back measurement.

The cross-section and side surfaces of the fibers were imaged by a scanning electron microscope (SEM; Philips XL30 field emission SEM) to study the surface defects.

The mechanical strength of the fibers was determined by measuring the fiber bending radius at fiber breakage (minimum bending radius) [29]. Fiber pieces of approximately 15 cm length were bent and held between two vertically parallel plates as shown in Fig. 2. One of the plates was held stationary, while the other was mounted to a movable rail driven by a stepper motor. The latter plate was set to move at a speed of 0.3 mm/s towards the fixed plate until fiber breakage. Measurements were repeated to estimate the minimum bending radius at least 10 times. The calculation of the strain was based on Eq. (3):

$$\tau_s = r/0.42D \quad (3)$$

where τ_s is the breaking strain which can be measured from D, the minimum distance between the plates when the fiber fractures, and r is the fiber diameter.

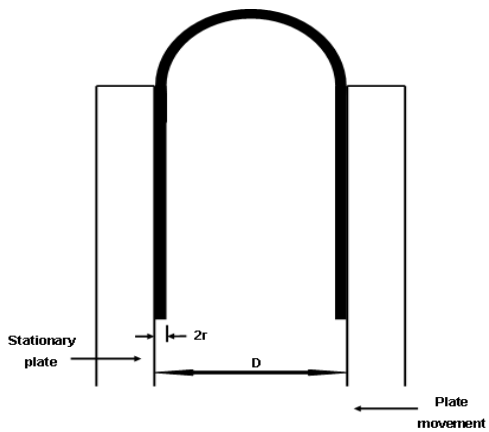

Fig. 2. Bending strength measurement approach.

#192346 - $15.00 USD Received 17 Jun 2013; revised 3 Aug 2013; accepted 4 Aug 2013; published 13 Aug 2013

3. Results and discussions

3.1 Optimization of glass melting

Table 1 lists the fluorination and melting conditions, and characteristic temperatures (T_g, T_x, and T_p) of samples A, B and C. The difference $\Delta T = T_x - T_g$ is used as a measure of glass stability.

Table 1. Melting conditions and properties of glass samples fabricated in this study.

Melting condition	Dwell Time @ 235 °C	Dwell Time @ 450 °C	Dwell Time @ 900 °C	T_g (°C)	T_x (°C)	T_p (°C)	ΔT (°C)
A*	45 min	---	3 h	307	385	409	78
B**	45 min	---	3 h	307	389	409	82
C**	---	1h	2 h	308	389	407	81

*raw material $InF_3 \cdot 3H_2O$ with~99.99% metal content
**raw material InF_3 with ~99.99% metal content

DSC measurements (Fig. 3, Table 1) show that different fluorination and melting conditions had negligible impact on T_g; the variations were within the temperature error of DSC measurements. However, it was found that Sample B contained a few un-dissolved particles. Mohammed [30] introduced 500 °C for elimination of NH_4HF_2 products prior to melting, for preparation of their fluoride glasses. Fluorination at 450 °C prior to melting in this work for Sample C may effectively reduce the remaining (i.e., non-reacted) NH_4HF_2 in the final glass. The un-dissolved particles in Sample B are attributed to possible residual products from NH_4HF_2 in the glass, which could not be eliminated by fluorination at 235 °C.

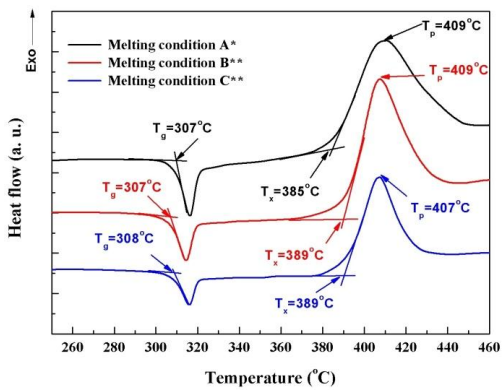

Fig. 3. DSC curves for glasses prepared under three different conditions.

Figure 4 shows the linear thermal expansion curve of the 5 mm diameter rod piece which was melted under the same condition as C** and extruded at 320 °C. The slope changes slightly at 308 ± 2 °C, which corresponds to the glass transition temperature (T_g). This value measured using a thermal dilatometer agrees well with the T_g value of the sample melted under condition C** (melted under the same conditions) obtained from DSC.

#192346 - $15.00 USD Received 17 Jun 2013; revised 3 Aug 2013; accepted 4 Aug 2013; published 13 Aug 2013

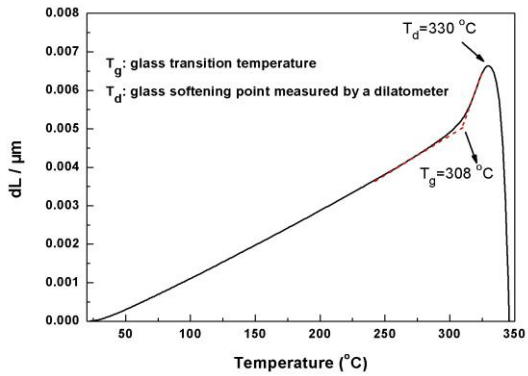

Fig. 4. Linear thermal expansion curve of IZSBGC sample obtained using 5 °C/min heating rate.

3.2 Extrusion

To achieve a good surface quality for glass items extruded through graphite dies, the extrusion force must be as low as possible while the temperature must be below the onset of glass surface crystallization temperature [9]. A low extrusion force minimizes shedding of graphite particles from the die onto the glass and reduces the chance of die breakage. Shedding can degrade the surface quality of extruded rods, whereas die breakage can lead to premature stopping of an extrusion trial. While higher temperatures decrease the extrusion force, they can increase the probability of the undesired surface crystallization. Therefore, the maximum temperature that can be used for extrusion of preforms with good surface quality will be limited by the onset of glass surface crystallization temperature.

For the IZSBGC fluoroindate glass, characteristic temperatures are around 307-308 °C for T_g and 385-389 °C for T_x (Table 1) depending on melting conditions. In our previous work [9], preliminary extrusion trials were conducted at 317 °C, 322 °C and 330 °C. In this work, to identify the best die design and advance our understanding of temperature-viscosity behavior and the impact of temperature on extrusion force and rod surface quality, we performed extrusion trials using different die designs and temperatures between 317 °C and 330 °C.

According to the previously published results [16,31,32], we can assume that the extrusion flow of fluoroindate glass follows the Poiseuille law, and that the glass can be regarded as a Newtonian fluid. Hence, the force or pressure required to extrude a glass through a circular die channel can be approximated by the following equation [16]:

$$P = \frac{128L_1}{\pi D_1^3 (D_1 + 8\alpha)} A_0 V_0 \eta \qquad (4)$$

where subscript '0' and '1' refer to the billet and die, respectively, $P = F/A_0$ is the pressure P calculated from the measured force F and billet cross section area A_0, L_1 is the die channel length, D_1 is the die channel diameter, V_o is the ram speed, η is the glass viscosity, and α is the slip coefficient at the glass/die boundary.

According to Eq. (4) and assuming a constant slip coefficient, the extrusion pressure is proportional to the die channel length and the inverse of the fourth exponent of the channel diameter. Metal dies made from stainless steel or nickel alloys were found to have no slip ($\alpha = 0$, i.e. constant slip coefficient) when they were used for the majority of oxide glass extrusions [16,32]. By contrast, graphite is a non-wetting material [32]. A slip at the glass/die boundary was observed previously by using graphite as an extrusion die material [16]. For extrusion of fluoroindate glass through graphite dies, we found that with the shorter die channel in die (c), compared to dies (a) and (b), the extrusion force did not decrease linearly

#192346 - $15.00 USD Received 17 Jun 2013; revised 3 Aug 2013; accepted 4 Aug 2013; published 13 Aug 2013

with the die channel length, L_1, which cannot be explained by Eq. (4) assuming a constant slip coefficient. Analysis of published data on extrusion of silicate glasses through graphite dies with different die channel length [16] revealed that the slip coefficient decreased linearly with decreasing die channel length, and can be approximated by:

$$\alpha(mm) = 0.5557 + 0.5652 L_1(mm) \quad (R^2 = 0.950) \tag{5}$$

Equation (5) indicates that α decreases with L_1. Therefore, the extrusion force decreases with L_1 in a nonlinear manner in Eq. (4), which explains our findings of the nonlinear decrease of the extrusion force with L_1 in the extrusion of fluoroindate glasses. Assuming that the dependence of die channel length on the slip coefficient for IZSBGC glass/graphite die interface is equal to that for silicate glass/graphite die interface, we used Eq. (5) to calculate the slip coefficients for different die channel length for our extrusion trials (Table 2).

Once the slip coefficient α is known, Eq. (4) can be used to calculate the viscosity from the measured extrusion force and other parameters in the extrusion trials conducted using different temperatures and graphite die geometries [16]. Table 2 shows the experimental parameters used for this calculation and the calculated viscosities. In Fig. 5, the calculated viscosity values are plotted as a function of the reciprocal of the glass temperature for fluoroindate glass extrusion trials, assuming die temperature is equivalent to glass temperature.

Table 2. Extrusion Parameters: Preform surface roughness, S_a and S_q, Extrusion temperature, T, Die Channel Diameter, D_1, Die Channel Length, L_1, Ram Speed, V_0, Ram Force, F, Ram pressure, P, Slip coefficient, α, Glass viscosity, η.[§]

Extrusion No	Preform surface roughness		Die Type	T (°C)	D_1 (mm)	L_1 (mm)	V_0 (μm/s)	F (kN)	α (mm)	log η (log Pa·s)
	S_a (nm)	S_q (nm)								
IE1	—	—	a	322	8	8	0.60	10.85	5.08	9.44 (± 0.06)
IE2	—	—	a	325	8	8	0.60	7.15	5.08	9.26 (± 0.04)
IE3	—	—	a	330	8	8	0.60	2.24	5.08	8.76 (± 0.03)
IE4	49.47 (± 5.68)	59.46 (± 10.83)	b	330	10	7	0.60	1.41	4.51	8.88 (± 0.04)
IE5	—	—	b	324	10	7	0.33	4.01	4.51	9.59 (± 0.05)
IE6	—	—	c	317	10	2	0.33	19.00	1.69	10.52 (± 0.03)
IE7	141.96 (± 14.22)	162.62 (± 6.96)	c	318	10	2	0.33	18.10	1.69	10.50 (± 0.03)
IE8	190.50 (± 10.90)	234.35 (± 21.65)	c	316	10	2	0.33	22.05	1.69	10.58 (± 0.03)
IE9	67.11 (± 7.20)	84.33 (± 7.61)	c	320	10	2	0.33	8.34	1.69	10.16 (± 0.05)
IE10	64.29 (± 1.88)	78.86 (± 0.96)	c	324	10	2	0.33	3.58	1.69	9.79 (± 0.04)
IE11	—	—	d	320	5	2	0.33	34.25	1.69	9.76 (± 0.06)

§: Note that only glass for IE11 was melted under condition C** and the glasses for IE1-10 were all melted under condition A*; the surface roughness S_a and S_q are the average values by repeating measurements 3 times.

#192346 - $15.00 USD Received 17 Jun 2013; revised 3 Aug 2013; accepted 4 Aug 2013; published 13 Aug 2013

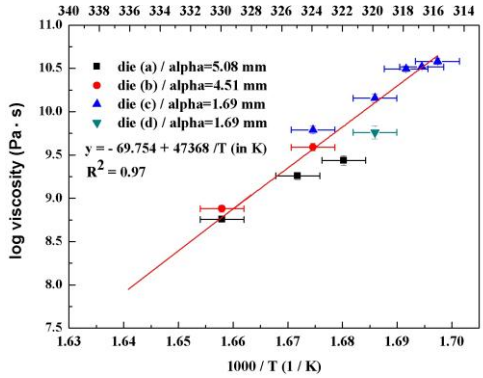

Fig. 5. Calculated viscosity values as a function of extrusion temperature.

For a limited viscosity range at the temperature between 317 and 330 °C, the experimental viscosity data can be well fitted with a two-parameter Arrhenius equation [31]:

$$log\eta = A + B / T \tag{6}$$

where η is the viscosity (in Pa·s), T is the temperature (in K) and A and B are empirical constants. For the fluoroindate glass reported in this work, we determined the Arrhenius equation of the temperature viscosity curve from glass viscosity calculated from extrusion trials. The linear fitting of Arrhenius equation for our fluoroindate glass yields $\log \eta$ (in Pa·s) = –69.754 + 47368/T (in K) (Fig. 5).

Using the dilatomer measurement (Fig. 3), the dilatometric softening temperature (i.e. the temperature, at which a sample reaches maximum expansion in a length versus temperature curve during heating of the sample [33]) was measured to be 330 °C for our fluoroindate glass. Note that the viscosity at this dilatometric softening temperature corresponds to 10^8-10^9 Pa·s [33], which is in agreement with the viscosity at 330 °C in Fig. 5, determined using the extrusion trials. This suggests the calculated viscosity results in Fig. 5 are reliable.

The surface roughness results for extruded preforms (Table 2) demonstrate that the roughness decreases with increasing extrusion temperature, which was also reported for extruded polymer preforms [34]. There are several reasons that possibly explain this observation. Firstly, the surface is smoothened by fire-polishing at elevated temperatures, i.e. at low glass viscosities [35]. The fire-polishing also occurs during extrusion. The glass preform is still hot when it emerges from the die exit and moves slowly out of the hot zone; this leads to fire-polishing of the preform surface. The fire-polishing process softens or melts the surface, which deliquesces and rounds sharp edges, and also fills pits (e.g., scratches) due to lower viscosity [36]. Consequently, the fire-polishing results in a smoothed preform surface and the surface roughness is reduced. The effects of fire-polishing will become more prominent with increasing temperature, thus leading to a smoother preform surface as the extrusion temperature increases.

Secondly, for a not completely wetted interface, a certain degree of slip occurs at the fluid/solid interface. For a Newtonian fluid, there exists a general nonlinear relationship between the amount of slip and the local shear rate at a solid surface [37]. The velocity gradient (shear rate) in viscous fluid flow generates a tangential force (mechanical shear stress) which is proportional to the viscosity when the fluid is under shearing [38]. When the temperature increases, the extrusion can be achieved at a lower viscosity with a lower shear stress. The lower shear stress, therefore, reduces the shearing at the graphite die surface, leading to reduced surface roughness and improved glass surface finish (e.g., less extrusion stripes). It also reduces the shearing of the graphite particles that can contaminate the glass surface, and therefore improves glass surface quality. Furthermore, higher extrusion forces can lead to

#192346 - $15.00 USD Received 17 Jun 2013; revised 3 Aug 2013; accepted 4 Aug 2013; published 13 Aug 2013

changes in the slip behavior at the fluid/die interface, which can result in melt fracture extrusion instabilities and increase the extruded preform's surface roughness [39]. Low extrusion forces at high extrusion temperatures are therefore desired to improve the surface roughness of extruded glass preforms.

Our recent work [9] on fluoroindate glass annealing tests demonstrated that a temperature of 330 °C for preform extrusion could cause potential surface crystallization, whereas 322 °C for extrusion was sufficiently low to avoid potential surface crystallization. Therefore, to achieve a low extrusion force and eliminate shear-induced surface roughness with no glass surface crystallization, we chose the extrusion temperatures of 320-322 °C for fiber drawing trials IF1-6 in the next section.

3.3 Fiber drawing

Table 3 summarizes the experimental details of fibers IF1-6 drawn under different conditions, and presents results of fiber surface roughness and fiber spot loss measurements at 1550 nm. To understand the surface roughness value of a fiber without surface crystallization, we also measured the surface roughness of an unstructured fiber made from commercial F2 lead-silicate glass for comparison (Schott Glass Co.) (Table 3). SEM analysis (Fig. 6) shows the features of the cross-sections and the surface of fibers IF1-6.

During fluoride fiber drawing, one of the most important aims is to minimize surface crystallization of the preform neck-down, because experiments have shown that this surface crystallization significantly correlates to degraded mechanical strength in the drawn fibers and increases fiber loss for air-clad (i.e., unstructured) fibers and air/glass microstructured fibers [28].

Chemical etching has been demonstrated to improve fluorozirconate glass surface quality and hence reduce surface crystallization [8]. Thus, we commenced with investigating the impact of etching on fluoroindate glass surface crystallization during fiber drawing. A preform extruded at 320 °C was cut into two pieces that were used for IF1 and IF2 fiber drawing trials using 2 cm heating zone. The difference between the two fiber drawing trials was that the IF2 preform was etched with 1.36 M $ZrOCl_{2(aq)}$ to remove a ~0.5 mm thick outer layer and then polished with 40 nm colloidal silica suspension, while the IF1 preform remained unetched. Surface roughness measurements of the IF2 preform before and after chemo-mechanical treatment revealed that the average roughness dramatically decreased from 70 to 7 nm (Fig. 7).

Table 3. Fiber drawing conditions, results of spot loss measurements and surface roughness of fibers IF1-6

Fiber No	Glass melting condition§	T (°C)	Surface treatment	Susceptor (cm)	Additional weight (g)	Fiber surface roughness		Spot loss at 1550 nm (dB/m)
						S_a (nm)	S_q (nm)	
IF1	A*	320	none	2	0	172.0 (± 77.0)	223.0 (± 103.0)	27.8
IF2	A*	320	Preform	2	0	149.0 (± 29.0)	205.0 (± 38.0)	20.1
IF3	C**	320	Preform	4.5	0	13.8 (± 4.1)	15.9 (± 4.4)	7.8
IF4	C**	320	Preform	4.5	190	10.5 (± 1.1)	15.2 (± 3.8)	4.1
IF5	C**	320	Billet/preform	4.5	190	9.3 (± 1.8)	12.9 (± 2.3)	3.6
IF6	C**	322	Billet/preform	4.5	190	9.1 (± 0.4)	12.8 (± 1.9)	2.3
F2† fiber	—	560	—	4.5	0	8.0 (± 0.8)	12.0 (± 1.2)	—

§: For glass melting conditions for IF1-6, please refer to Table 1.

†: Commercial F2 glass billet (outer diameter: 30 mm) was used to fabricate extruded preform and unstructured fiber.

#192346 - $15.00 USD Received 17 Jun 2013; revised 3 Aug 2013; accepted 4 Aug 2013; published 13 Aug 2013

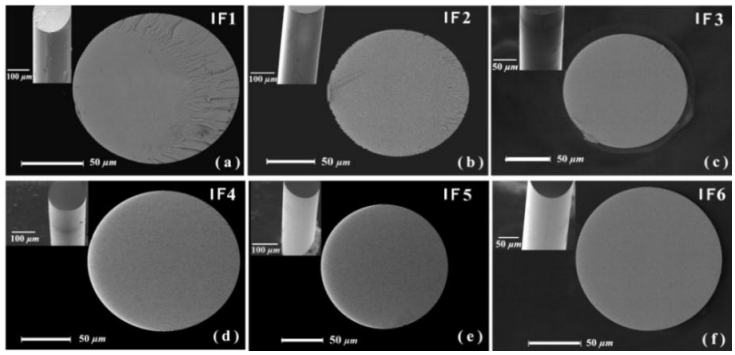

Fig. 6. Scanning electron microscopy images of fiber surfaces and cross-sections (IF1-6).

To investigate the effect of the chemo-mechanical treatment on the preform during fiber drawing, IF1 and IF2 preform neck-down surfaces were examined under an optical microscope (Fig. 8). During fiber drawing, re-heating of the IF1 preform resulted in the formation of corrugation patterns on the surface of the preform neck-down (Fig. 8(a)). This corrugation pattern is attributed to surface crystallization during glass re-heating. In contrast, no corrugation patterns were observed on the IF2 preform neck-down (Fig. 8(b)) except for several small crystal spots on the surface. The fiber surface roughness of IF2 was reduced to 149 ± 29 nm (S_a), as compared to 172 ± 77 nm (S_a) for IF1 (Table 3). This clearly indicates that the chemo-mechanical treatment applied to IF2 preform effectively reduced surface crystallization during fiber drawing.

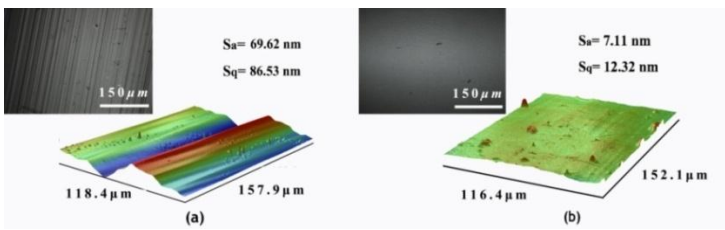

Fig. 7. Optical interferometric profiler images (colored images) of preform surface for IF2 fiber drawing (a) before chemo-mechanical treatment; the data in (a) is one of the measurements used for the surface roughness calculation of IE9 preform, Table 2; (b) after chemo-mechanical treatment. Images in grey scales in (a) and (b) are optical microscope images of the preform surfaces before and after chemo-mechanical treatment.

In Fig. 6, all the fibers from IF1 to IF6 were cleaved at a tension as low as possible to prevent a mirror-mist hackle pattern, which was otherwise observed to occur at high tensions. In addition, each fiber was cleaved at least 20 times to ensure that fiber surfaces (Fig. 6) were reproducible and representative. For all the cleaved surfaces of IF1, the fiber cross-section shows fracture patterns that resemble a mirror-mist hackle pattern (Fig. 6(a)). It is likely that this fracture pattern arises from surface crystallization and propagated rapidly when the fiber is fractured [8]. For IF2 fiber, its preform was chemo-mechanically treated before fiber drawing, resulting in significantly reduced mirror-mist hackle pattern (Fig. 6(b)).

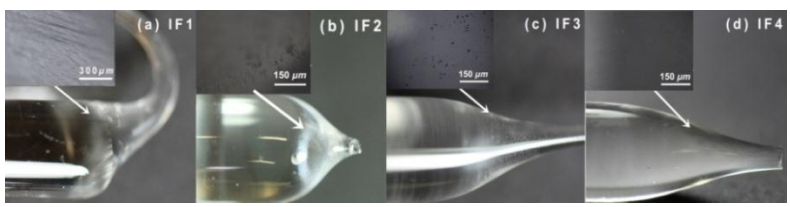

Fig. 8. Surface images of the fiber drop neckdown of IF1-4.

#192346 - $15.00 USD Received 17 Jun 2013; revised 3 Aug 2013; accepted 4 Aug 2013; published 13 Aug 2013

For the IF2 fiber, surface crystallization was reduced but not completely suppressed, as demonstrated by observation of crystal spots on the preform neck-down. Sakaguchi et al. [28] successfully minimized surface crystallization in the neck-down region of a fluorozirconate glass by extending the heating zone of the furnace used for fiber drawing. As fluoride glass has a steep temperature-viscosity dependence, small temperature fluctuations cause large variations in the glass viscosity. Thus, instabilities in drawing such as variations in diameter (± 30 μm for IF2) and drawing tension are caused by a shorter heating zone with a higher maximum preform temperature and steeper preform temperature gradient along the drawing axis [28]. The steeper temperature gradient requires higher maximum glass temperature to form a preform drop, which may lead to an increase in surface crystallization. In contrast, for a longer heating zone, the reduced temperature gradient and larger heat spread in axial direction allows the preform to drop at a lower maximum temperature, which reduces the probability of surface crystallization during fiber drawing. The neck-down shape using a longer heating zone is elongated, which indicates that the duration time for glass in the heating zone is increased compared to that of a shorter heating zone. The reduction of surface crystallization for a longer heating zone indicates that the impact of temperature on crystallization is more significant than the time the glass dwells in the hot zone [28].

For our fiber drawing furnace, we have confirmed that the susceptor length correlates with the length of the heating zone. To investigate the impact of increased heating zone length on surface crystallization for our fluoroindate glass fibers, we used a larger susceptor length of 4.5 cm for IF3 compared with 2 cm-long susceptor for IF2. IF3 was drawn at a furnace temperature being ~75 °C lower than that of IF2. This confirms that, for a longer heating zone, a lower maximum temperature can be used to form a preform drop. The length of neck-down of IF3 was observed to be elongated compared to that of IF2 (Fig. 8), consistent with results by Sakaguchi et al. [28], indicating lower maximum glass temperature. Although the neck-down surface of IF3 contained similar small crystal spots compared with those of IF2 (Fig. 8), the number of spots was significantly reduced. SEM images revealed that the mirror-mist hackle patterns of IF3 were greatly suppressed (Fig. 6(c)). In addition, the fiber surface roughness (S_a) was reduced from 149 ± 29 nm for IF2 to 13.7 ± 4.1 nm for IF3 (Table 3). These results demonstrate a decrease in surface crystallization for IF3, due to the reduced maximum preform temperature of IF3 combined with reduced temperature gradient along the drawing axis as a result of the longer heating zone used for IF3 than that for IF2.

For IF4, we applied an additional weight at the bottom of its preform to decrease the preform temperature required to form a drop during fiber drawing. The decreased preform temperature also reduced the surface crystallization rate (without wasting a significant length of the preform). The fiber drop temperature for IF4 decreased by 15 °C in comparison with IF3. No crystallization was found on the neck-down of IF4 on inspection with an optical microscope (Fig. 8 (d)). Both surface roughness of IF4 (Table 3) and mirror-mist hackle patterns of cleaved fiber cross-section (Fig. 6) were reduced due to the reduced crystallization of the fiber surface. Note that all billets for IF1-4 were polished mechanically.

For comparison, chemo-mechanical treatment was applied to IF5 and IF6 billets before extrusion. The only difference between IF5 and IF6 was that the preforms for these two fiber drawing trials were extruded at different temperatures (320 °C for IF5 and 322 °C for IF6). By comparing the fiber surface roughness of IF4 and IF5, we find that the chemo-mechanical treatment of IF5 billet before extrusion slightly improved the IF5 fiber surface quality and resulted in a reduced surface roughness relative to IF4 (Table 3). The improved fiber surface quality of IF5 is attributed to an improved billet surface quality after chemo-mechanical treatment, superior to use of only mechanical billet polishing before extrusion (for IF1-4). Chemo-mechanical treatment of the billet for IF5 removed surface micro-cracks and micro-scratches before extrusion, thereby enabling IF5 to have a lower fiber surface roughness. IF6, which was fabricated from a preform extruded at 322 °C, exhibits the lowest surface roughness (Table 3) of all fluoroindate fibers fabricated, and no mirror-mist hackle

#192346 - $15.00 USD Received 17 Jun 2013; revised 3 Aug 2013; accepted 4 Aug 2013; published 13 Aug 2013

patterns were found on this fiber cross-section (Fig. 6(f)). It is also the longest fiber obtained in this work with a length of 38 m. These results are attributed to the better surface quality of the IF6 preform by extruding the preform at 2 °C higher than those used for extrusion of IF1-5, resulting in a lower force for extrusion of IF6 preform. As discussed above, lower force results in an improved preform surface quality, which finally leads to improved fiber surface quality.

The spot loss measurement results at 1550 nm shown in Table 3 and Fig. 9 are consistent with the broadband fiber loss measurement results (Fig. 9). Note that no fiber of IF1 with adequate length was available for broadband loss measurements to be performed after spot loss measurement, due to low production yield of this fiber. The broad absorption band at 1000 nm of IF2 (Fig. 9) is thought to be due to absorptions from 3d transition metals (e.g., Fe^{2+}, Co^{2+}, Cu^{2+}) from the raw materials used for IF2. Both spot loss and broadband fiber loss results demonstrate that the loss is remarkably decreased from IF1 to IF6, which correlates with reduction of the fiber surface roughness. As IF1 and IF2 were made from the same billet and preform, the lower loss of IF2 compared with IF1 demonstrates that the loss is determined by surface scattering due to surface roughness caused by surface crystallization. Similar correlation is observed for IF3 to IF6 made from glass using C** melting condition. The reduction of surface crystallization from IF1 to IF6 resulted in a smooth fiber surface with low surface roughness, which effectively reduced light scattering and thus fiber loss.

IF6, which has the lowest loss in the near-infrared region of all fibers investigated in this work, also exhibited low loss in the mid-infrared region; the fiber loss of IF6 at 2, 4, 5 μm was measured to be 2.0, 1.5 and 2.2 dB/m, respectively. The lowest loss of 1.3 dB/m was located at 2.7 μm. In comparison, an unstructured ZBLAN fiber, which was made using commercial raw materials with comparable purity, fluorination with NH_4HF_2 at 235 °C, identical controlled atmosphere melting facility and the extrusion technique for preform fabrication, demonstrated a similar fiber loss of 1.1 ± 0.5 dB/m at 4.0 μm [20].

A 2 m-long fiber with 1.9 dB/m fiber loss at 1550 nm was drawn from an un-etched preform in our previous work [9], while IF6 with 2.3 dB/m was obtained with a length of 38 m. The significantly larger fiber yield for IF6 is attributed to the higher fiber drawing stability achieved. This is believed to be due to the improvements in the fiber fabrication conditions, resulting in the suppression of fiber surface crystallization during fiber drawing. Although chemical etching and additional weight were applied to prevent crystallization during fiber drawing in this work, IF6 exhibited a slightly higher fiber loss of 2.3 dB/m compared to the previously obtained fiber with 1.9 dB/m [9]. This can be explained by the relatively high levels of impurities in the raw materials used in this work: ZnF_2 - this work: 99%, work in [9]: 99.9%; and BaF_2 - this work: 99.99%, work in [9]: 99.999%. Those high purity raw materials used in our previous work are no longer available for purchase.

To further study the correlation between fiber loss and surface roughness, we also measured the fiber surface roughness of an unstructured F2 soft glass fiber. Ref [18]. demonstrated that the loss of air-clad and air/glass microstructured fibers was dominated by surface scattering associated with surface roughness compared with the loss of the bulk material, and that extruded F2 glass fibers showed the same loss as that of the F2 bulk glass within the measurement errors. This indicates that the surface roughness of unstructured F2 fiber is so low that it does not contribute to fiber loss. The indium fluoride fiber IF6 shows a surface roughness of 9.1 ± 0.4 nm (S_a), which is very close to the F2 fiber surface roughness of 8.0 ± 0.8 nm (S_a). This result confirms that the reduced surface roughness from IF1 to IF6, due to reduced surface crystallization, leads to a decrease in light scattering and hence reduces fiber loss both in spot loss and broadband fiber loss measurements.

The fiber breaking strains gradually increased from IF1 to IF6 (Table 4 and Fig. 10), which correlates with the observed decrease in fiber surface roughness (Table 3). A smooth fiber surface without defects (e.g. crystals) is, unsurprisingly, an important characteristic of high strength fibers [28]. The enhanced breaking strain of the fibers from trial IF1 to IF6 is

#192346 - $15.00 USD Received 17 Jun 2013; revised 3 Aug 2013; accepted 4 Aug 2013; published 13 Aug 2013

attributed to the reduced surface roughness due to the reduced crystallization on the fiber surfaces during fiber drawing via improvement of the preform and fiber fabrication conditions.

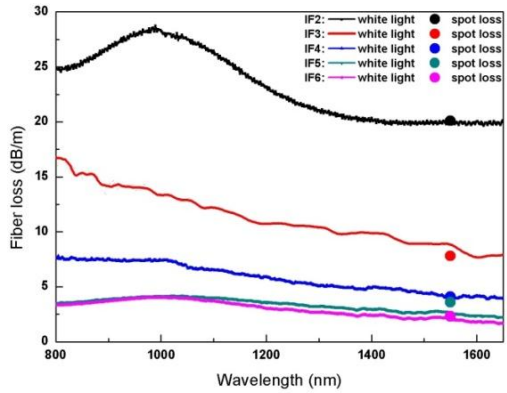

Fig. 9. Fiber loss spectra and spot loss measurement results at 1550 nm of IF2-6.

Table 4. Fiber strain of Trial IF1-6

	IF1	IF2	IF3	IF4	IF5	IF6
Mean of measured radius (μm)	62.34	83.23	71.85	84.28	88.25	77.21
Mean of calculated strain (10^{-3})	4.49	4.94	5.59	6.21	7.43	10.54
The standard deviation of calculated strain (10^{-3})	1.90	1.69	1.34	1.10	0.93	0.79

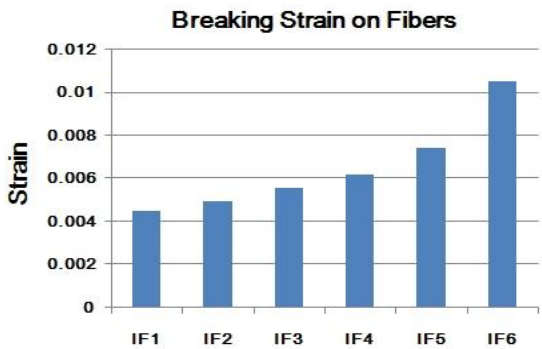

Fig. 10. Breaking strain of IF1-6.

4. Conclusions

We have presented a systematic characterization of factors responsible for scattering loss in fluoroindate glass fibers. The results showed that this systematic refinement of the glass and fiber fabrication processes reduced the fiber loss by an order of magnitude: from 27.8 dB/m to 2.3 dB/m. This improvement is attributed to the reduction in fiber surface roughness achieved by optimizing the melting, preform and fiber fabrication conditions.

Sample C melted using anhydrous InF_3 raw material with higher fluoride content demonstrated a higher glass crystallization stability compared to Sample A melted using $InF_3 \cdot 3H_2O$ raw material. High fluorination temperature of 450 °C for sample C enabled successful preparation of a crystal-free glass and eliminated the remaining NH_4HF_2 in the glass.

The preform surface properties including surface roughness and crystallization of extruded fluoroindate glass rods essentially depended upon the extrusion temperature. A relatively high temperature reduced the extrusion force, which minimized graphite shedding, cracking of dies and slip instabilities between glass and die surface. The fire-polishing effect became prominent

#192346 - $15.00 USD Received 17 Jun 2013; revised 3 Aug 2013; accepted 4 Aug 2013; published 13 Aug 2013

with increasing temperature, thus leading to a smoother preform surface as the extrusion temperature increased. Both these effects were found to be essential to minimizing rod surface roughness. However, even for rods with good surface finish, sufficiently high temperature eventually resulted in surface crystallization. In this study, the optimum temperature for extrusion was found to be around 322 °C.

The maximum fiber drawing temperature was reduced by expanding the length of the heating zone in the drawing furnace. The chemo-mechanical treatment of billets and preforms reduced the surface crystallization observed on the preform neck-down and fibers at the elevated temperatures experienced during fiber drawing. Surface crystallization was completely suppressed by using additional weight at the bottom of preforms.

In conclusion, the fiber surface roughness due to surface crystallization was reduced by optimizing the preform and fiber drawing conditions (including the extrusion temperature; chemo-mechanical treatment; expanding the heating zone length to decrease the maximum preform temperature; additional weight). This also reduced the loss of the fabricated fibers and the increased fiber strength from trial IF1-6. Furthermore, the improved fiber drawing conditions significantly increased the yield of low-loss fiber (~1.5 dB/m at 4 μm wavelength in the mid-IR region) from a 2 m achieved in our previous work [9] to 38 m for IF6 in this work. However, the fluoroindate fiber IF6 has a significantly lower fiber loss of 1.8 dB/m at 4.7 μm. This is because that fluoroindate glasses have longer multi-phonon edge wavelengths (> 4.7 μm) [9] compared to ZBLAN (<4.7 μm) [20].

In addition to extrinsic scattering loss in fluoroindate glasses discussed above, extrinsic absorption loss is another factor causing high fiber loss. As commercially available fluoride raw materials often contain transition metals and oxides impurities, it limits the reduction of extrinsic absorption loss in fibers [40]. Sublimation and distillation techniques are established methods of purification for high-purity fluorides [40]. In the future, we will aim to quantify the contributions of both extrinsic scattering and absorption to IZSBGC glass fiber loss to determine which one is the major contribution. This future work will guide us to the pathways for further improvement of the fabrication conditions.

Acknowledgment

We acknowledge support from Defence Science and Technology Organisation (DSTO) for funding this work. We also acknowledge the facilities, and the scientific and technical assistance of the Australian Microscopy & Microanalysis Research Facility at Adelaide Microscopy Centre of The University of Adelaide. This work was performed in part at the Optofab node of the Australian National Fabrication Facility, a company established under the National Collaborative Research Infrastructure Strategy to provide nano and microfabrication facilities for Australia's researchers. We thank Mr Roger Moore (University of Adelaide) for fiber drawing, Johann Troles (Université de Rennes 1) and Jonathan Campbell (The Flinders University of South Australia) for DSC measurements and Dr. Yinsheng Xu & Dr. Xunsi Wang (Ningbo University) for the thermal dilatometer measurement. Jiafang Bei acknowledges the International Postgraduate Research Scholarship (IPRS) and discipline of physics supplementary scholarship supported by The University of Adelaide. H. Ebendorff-Heidepriem acknowledges the support of a DSTO Fellowship and T.M. Monro acknowledges the support of an ARC Federation Fellowship.

#192346 - $15.00 USD Received 17 Jun 2013; revised 3 Aug 2013; accepted 4 Aug 2013; published 13 Aug 2013